Theoretical Study of the Mechanisms of Ethylene Polymerization with Metallocene-Type Catalysts

L. Petitjean,[†] D. Pattou,[†] and M. F. Ruiz-López*,[‡]

Groupement de Recherches de Lacq, Elf-Atochem, BP 34, 64170 Artix, France, and Laboratoire de Chimie Théorique,[§] UMR CNRS-UHP 7565, Université Henri Poincaré, Nancy I, BP 239, 54506 Vandoeuvre-les-Nancy Cedex, France

Received: July 10, 1998

Three possible mechanisms of ethylene polymerization in the presence of zirconocene catalysts have been described through density functional calculations. About 20 structures (reactants, intermediates, transition states, and products) have been located on the potential energy surface. Only two mechanisms, called frontside and stepwise backside, appear to be competitive. The frontside mechanism has already been described in the literature, but we present here some important new aspects. In particular, we discuss the important role of the perpendicular form of the olefin π-complex for the frontside process. The stepwise backside mechanism is reported for the first time. The energy barriers in both mechanisms are on the order of 3 kcal/mol, which is compatible with the experimental and theoretical values available for similar processes. The energy difference between both mechanisms is certainly below the computational method accuracy, and a definitive conclusion regarding the most favorable mechanism cannot be drawn. The influence of other factors such as substituents on the catalysts or the size of the polymer chain could be fundamental.

1. Introduction

Transition-metal catalysis for the polymerization of α-olefins is one of the most important applications of organometallic chemistry in industry. Since the discovery in the 1960s by Ziegler[1] and Natta[2] of $TiCl_4/AlEt_3$ catalysts supported on $MgCl_2$, a substantial amount of research has been directed toward the understanding of the insertion and chain propagation mechanisms. In early works, the lack of knowledge about the structure of the active species had restrained the investigations to the exploration of two main mechanisms, proposed by Arlman and Cossée[3−5] and by Brookhart and Green[6] (Scheme 1). However, since the discovery of metallocene/MAO homogeneous catalysts by Kaminsky[7] in the 1980s and the recent development of Ni(II) and Pd(II) catalysts,[8−10] much experimental and theoretical work has been devoted to these processes and many advances have been achieved.[11] In particular, the cationic nature of the active species has been elucidated.[12−14] Despite this substantial research effort, the mechanism of olefin polymerization with metallocene catalysts is still incompletely known and deserves further work.

Theoretical calculations are expected to simplify the analysis and interpretation of the experimental findings and also to be of valuable assistance in the design of new catalysts exhibiting improved properties. Obviously, the large size of the systems involved in these kinds of processes renders extremely difficult their study through full accurate quantum mechanical calculations, especially considering the fact that accounting for correlation energy is in general necessary to correctly describe the properties of metal-containing complexes. Hybrid quantum mechanics/molecular mechanics (QM/MM) techniques are presently being developed[15] and have been already employed to study some catalyzed processes,[16] although much work is still necessary in particular to ameliorate the treatment of the QM/MM frontier atoms. Another possible approach consists of the study of model systems through quantum mechanical methods, and indeed, many applications of this type have been reported for the mechanism of olefin polymerization.[17−56]

In particular, Ziegler and co-workers have published a series of papers within the framework of the density functional theory (DFT) approach, using basically the local density approximation (LDA).[44−55] These authors have considered the mechanism of reaction between an ethylene molecule and an active species modeled either by $[Cp_2ZrEt]^+$ or by the constrained-geometry catalyst $[(Cp(SiH_2)NH)Ti(R)]^+$ species. They have shown that several conformations are possible for the polymer in the resting-state complex corresponding to α-, β-, γ-, or δ-agostic interactions,[57,58] as represented in Chart 1. The β-H agostic structure is substantially more stable than the others, and therefore it is supposed to correspond to the resting state (i.e., the species formed between two insertions of an ethylene monomer). Starting from the β-H agostic complex and an ethylene molecule, the reaction proceeds through the formation of a π-complex between the active species and the olefin. This may be occur via two different orientations, syn and anti, depending on the relative position of the olefin with respect to the H atom involved in the β-agostic interaction. Each complex leads to the final product through different reaction paths which are summarized in Scheme 2. The reaction mechanisms corresponding to syn and anti complexation are called the frontside (FS) and backside (BS) mechanisms, respectively. As shown in Scheme 2, in the FS mechanism, the growing chain must undergo a rotation so that the α-carbon atom is able to interact with the incoming olefin. This rotation is expected to lead to an α-agostic complex, although such a structure could not be obtained after full geometry optimization, the minimization procedure leading directly to the product.[51] The rate-limiting

[†] Elf-Atochem.
[‡] Université Henri Poincaré.
[§] Part of the Institut Nancéien de Chimie Moléculaire.

10.1021/jp982976s CCC: $18.00
Published on Web 12/12/1998

SCHEME 1

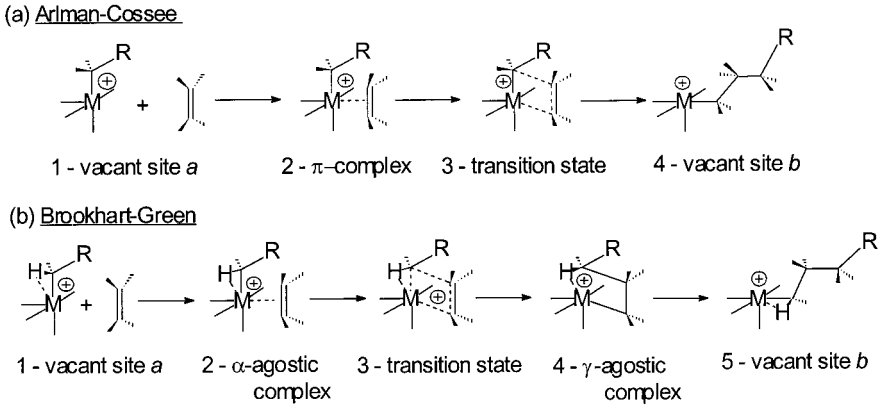

CHART 1

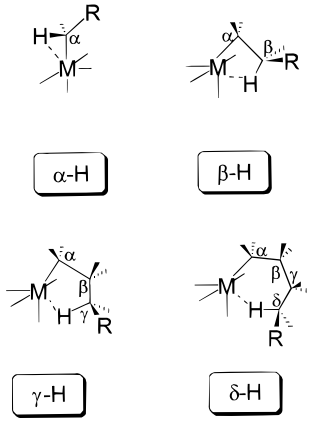

SCHEME 2

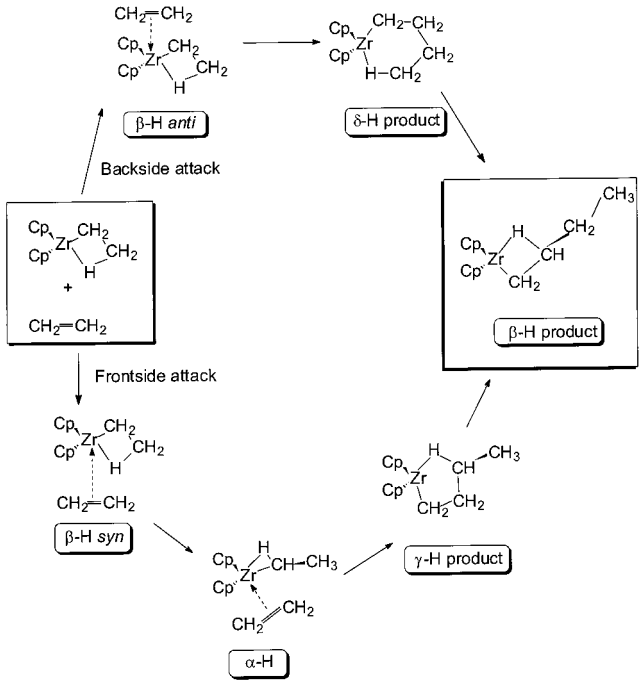

step in the FS mechanism was predicted to be polymer reorientation, the insertion being practically barrierless. In the case of the BS mechanism, the insertion can be made directly, without any rotation of the polymer chain. This process, however, was predicted to have a larger energy barrier than that for the rotation step in the FS mechanism, and as a consequence, the FS mechanism was predicted to be the most favorable one.

Ab initio computations have also been carried out for similar reactions by Morokuma and co-workers.[37−43] In particular, Yoshida et al.[40] have reported a study on ethylene polymerization with silylene-bridged metallocene catalysts. Activation energies were in good agreement with available experimental data. A comparison of MP2 and DFT results was also made showing that both approaches lead to close structures. Nevertheless, since the polymer chain in the active species was modeled by a methyl group, the important stabilizing role of β-agostic interactions was ignored.

Molecular dynamics studies using the Car−Parrinello approach have also been reported.[21,23,52] Margl et al.[52] have evaluated free energies of activation for selected reaction paths corresponding to the work of Lohrenz et al.[51] Such a study represents a substantial contribution to the understanding of the mechanism, in particular through the evaluation of characteristic times (for instance for the lifetime of agostic interactions). This type of simulation is still quite computer time demanding, and only a small number of trajectories may be simulated so that statistical averaging is difficult to achieve.

In the present work, we have revisited the mechanisms of ethylene polymerization with metallocene catalysts. Our main goal was to obtain a better characterization of the potential energy surface than in previous works and to discuss other possible mechanisms not yet explored in the literature. For this purpose we used a DFT approach with gradient-corrected exchange-correlation functionals and full geometry optimization at that level. Transition structures were rigorously located on the potential energy surface. As in previous studies,[51] the polymer chain was represented by an ethyl unit, so that β-agostic interactions in the active species, $[Cp_2ZrEt]^+$ in our case, were considered.

2. Calculations

The present calculations were carried out using the density functional theory approach and the Gaussian 94 package.[59]

The basis set D95[60] was employed for C and H atoms. For Zr, a double-ζ basis set together with Los Alamos effective core potentials (ECPs)[61−63] for the description of core electrons was used. All calculations were performed with the BLYP exchange-correlation functional.[64] The BLYP functional uses an LDA approximation with gradient corrections for the exchange functional, as proposed by Becke,[64a] and for the correlation functional, as proposed by Lee, Yang, and Parr.[64b]

All the geometries were fully optimized without any constraints or symmetry conditions. It should be noticed that the Cp rings may adopt an eclipsed or a staggered conformation. Though it was not possible to make a systematic study of Cp

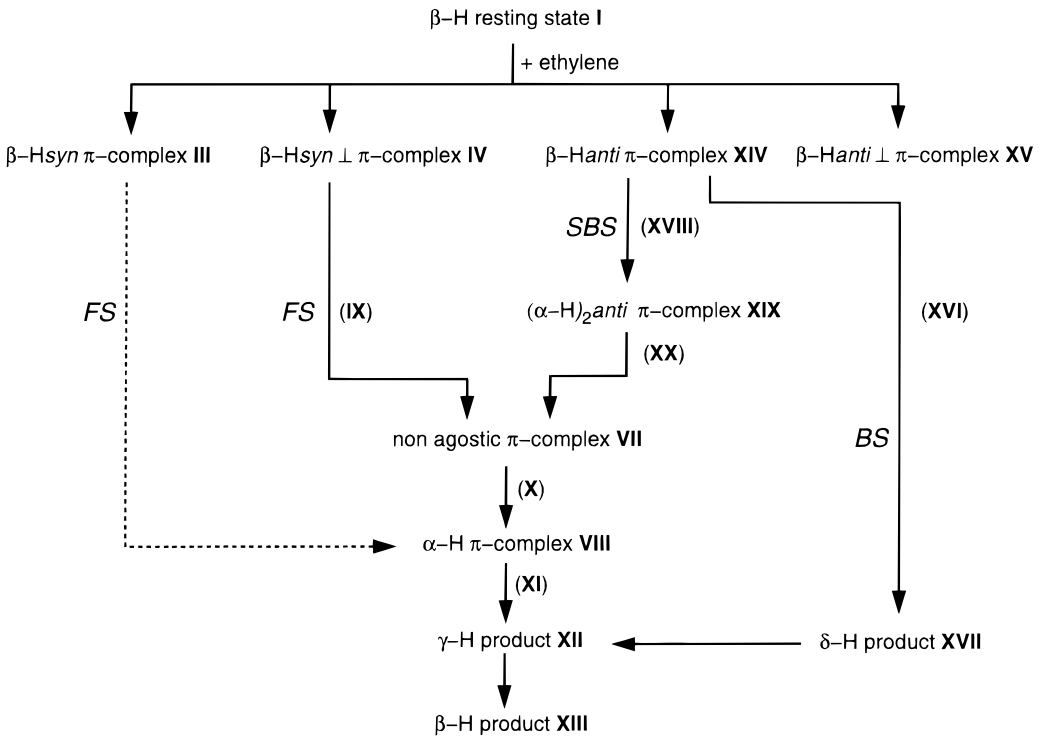

Figure 1. Structures involved in the three pathways predicted by our computations. Transition structures are given in parentheses. The frontside mechanism previously proposed by Ziegler and co-workers[50] is indicated by a dashed line (FS = frontside, BS = backside, SBS = stepwise backside).

conformation for all the structures presented in this work, we tested in a few cases that only one conformation leads to an energy minimum or a saddle point. For optimizations to a transition structure, we used the QSTN method.[65] Due to the large size of the present computations, no frequency calculations were possible after the geometry optimizations. Since many of the structures described here are similar to those characterized by Lohrenz et al.[50] at a lower level, we may reasonably conclude that the stable structures and transition structures obtained in our work correspond to true minima and saddle points on the potential energy surface. Though an incoming version of the Gaussian package analytic second derivatives of the ECPs were included, frequency computations were still too expensive. The calculations were done on an SGI R10000 processor. A cycle of geometry optimization required typically 120 min of CPU.

We first discuss the geometrical parameters obtained for the relevant structures; then, we consider the reaction energetics.

3. Mechanisms of Reaction

As pointed out in the Introduction, we focus this study on the potential energy surface description for the reaction of ethylene with the cationic active species. We first examined the FS and the BS mechanisms proposed in the literature and represented in Scheme 2. As we show below, we found substantial differences with respect to previous computations. Thus, whereas the BS mechanism was quite close to that reported by Lohrenz et al.,[51] new structures were located on the potential energy surface in the FS mechanism. In particular, a very weak α-agostic structure is described which appears to play a fundamental role in the reaction mechanism. Moreover, our results tend to indicate that there is no transition structure directly connecting the β-H syn and the α-H structures reported previously[50] for the reaction.

Apart from the FS and BS mechanisms, we examined for the first time another reaction path that will be called hereafter the stepwise backside mechanism (SBS). In this case, the olefin is initially coordinated to the β-agostic resting species, as in the BS mechanism; that is, the β-H anti complex is the starting species. In the BS mechanism, this complex gives the products through direct insertion in a single-step process. In the SBS mechanism, the β-H anti complex undergoes a chain rotation to form a weak α-agostic structure which is exactly that mentioned above for the FS mechanism, so that the remaining steps to yield the product are similar in the FS and SBS mechanisms.

The intermediates and transition structures predicted by our computations in the three proposed reaction mechanisms are summarized in Figure 1.

3.1. Resting State. We found two possible arrangements for the resting state corresponding to α-H and β-H structures. Attempts to find other conformations of the resting state with two β-H agostic interactions through a rotation of the chain methyl group, as already suggested,[36,49] were unsuccessful. The located structures are shown in Figure 2. We describe here both structures for comparative purposes, but one must keep in mind that the α-H agostic structure is considerably less stable than the β-H one (see Lorhenz et al.[51] and energies below). Hence, it will not be considered for the reaction mechanisms.

The β-H initial structure (**I**) exhibits a strong agostic interaction with a Zr−H_{ag} distance of 2.217 Å. The Zr−C_α−C_β−H_{ag} cycle adopts a planar conformation so that the complex has C_s symmetry (we use the notation H_{ag} for the hydrogen atom involved in the agostic bond). This arrangement is sterically favored by minimizing the interactions between the chain and the cyclopentadienyl (Cp) ligands.

In the α-H conformation (**II**) of the resting state, the Zr−H_{ag} distance (2.313 Å) is roughly 0.1 Å longer than that for the β-H complex. The Zr−C_α−H_{ag} ring is very constrained (Zr−C_α−H_{ag} = 79°) as expected for this bond type.[66] Besides, because the ethyl group lies out of the middle plane, there are

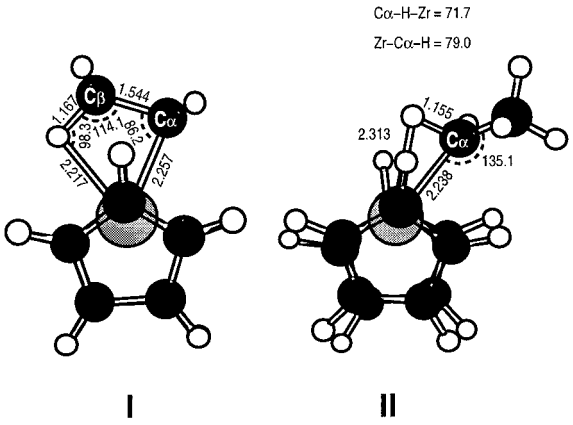

Figure 2. Conformations of β-H (**I**) and α-H (**II**) resting states.

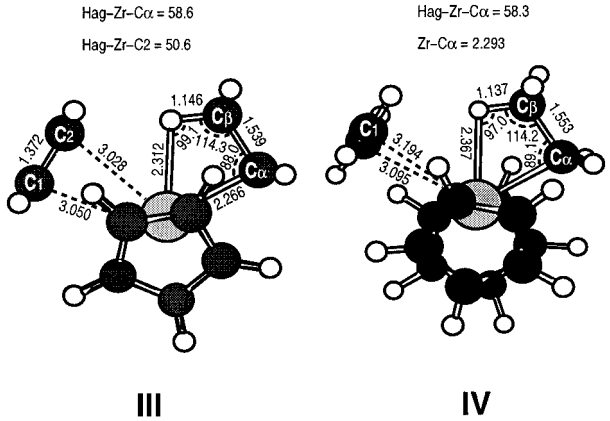

Figure 3. Main possible starting π-complexes for the FS mechanisms of β-H syn (**III**) and β-H syn $\perp$ (**IV**).

strong steric repulsions between this group and the Cp ligands, so that Zr−C_α−C_β angle is quite large (135.1°).

3.2. Frontside Mechanism (FS). *Complexation.* In principle, two possible complexes can be formed in the syn attack of the olefin on the β-H resting state **I**, depending on the orientation of the olefin with respect to the original symmetry plane. Thus, in-plane and perpendicular coordinations have been obtained, as represented in Figure 3, called hereafter β-H syn (**III**) and β-H syn $\perp$ (**IV**), respectively. Only one of these complexes (**III**) has been envisaged by Lohrenz et al.[50] for the calculation of the FS mechanism.

In **III**, the Zr, C_α, C_β, and H_{ag} atoms remain roughly in the plane after complexation. Moreover, the olefin carbon atoms also lie in this plane so that the symmetry of the structure is roughly C_s. If one compares the geometry of **III** with that of the β-H resting state **I**, one sees that the metal−carbon and metal−hydrogen distances increase. This may be due, at least in part, to electron donation from the monomer which tends to weaken the metal−chain bonds. However, steric interaction between the monomer and the chain may also be invoked.

In **IV**, the olefin is coordinated perpendicularly to the approximate symmetry plane. The planarity of Zr−C_α−C_β−H_{ag} is lost (Zr−C_α−C_β−H_{ag} = 11.9°), and the Zr−H_{ag} distance is substantially larger than that in the resting state **I**. The olefin is not exactly symmetrically coordinated (Zr−C_1 = 3.194 Å and Zr−C_2 = 3.095 Å), and the complexation is weaker than that for the β-H syn complex **III**. Steric repulsions between the olefin and the chain and between the olefin and the Cp ligands could explain these features.

Other minima were found (**V** and **VI**; see Figure 4) through rotation of the methyl group in **III** and **IV**. Such a conformation

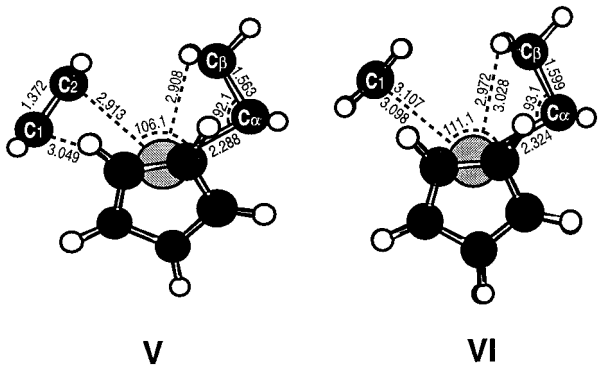

Figure 4. Structures of (β-H)$_2$ syn (**V**) and (β-H)$_2$ syn $\perp$ (**VI**) complexes.

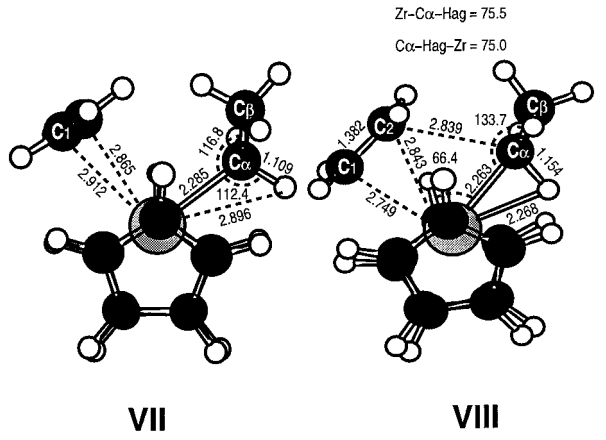

Figure 5. Structures of α-H π-complexes: α-H $\perp$ (**VII**) and α-H (**VIII**).

of the chain has already been described for the resting state,[36,49] but as we pointed out, we did not find it at the present computational level. Complexes **V** and **VI** are less stable (see below) than **III** and **IV**, respectively, and may be simply considered as rotamers of these complexes.

Chain Rotation. In the FS insertion mechanism described previously through LDA calculations,[51] chain rotation in the β-H syn complex to form an α-H complex is required prior to the insertion step. However, in these calculations,[51] the α-H structure could not be obtained after full geometry optimization. For this reason, the process going from the β-H to the α-H was described using geometry constraints, which prevented the spontaneous formation of the product in the energy minimization procedure.[51] Thus, a crucial point which deserves further investigation is the possible existence of a stable α-H structure on the potential energy surface as well as the nature of the transition state connecting the starting β-H syn complex with the α-H species. Within this scope, we carried out a series of full geometry optimizations starting from β-H syn complexes for different initial values of the chain dihedral angle. In this way, two α-H structures were located, **VII** and **VIII**, which are plotted in Figure 5.

In structure **VII**, the olefin presents nearly perpendicular coordination with a difference in metal−carbon distances of about 0.05 Å. In this complex, the α-agostic interaction seems to be rather small. On one hand, the Zr−H_{ag} distances are 2.896 Å (for the in-plane H atom) and 2.755 Å (for the out-of-plane H atom), which are substantially longer than the distance in the other α-H complex **VIII** (2.268 Å), for instance. On the other hand, the C_α hybridization is not far from the standard tetrahedral sp^3, as shown by the angles Zr−C_α−C_β (116.8°) and Zr−C_α−H (112.4 and 102.8°).

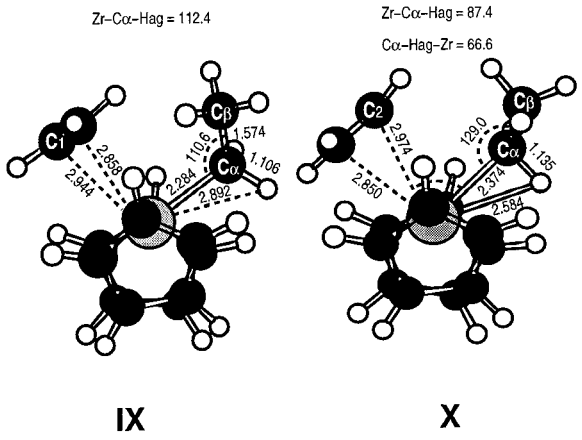

Figure 6. Transition structures located along the FS mechanism for chain rotation (**IX**) and olefin rotation (**X**).

In **VIII**, the olefin is slightly asymmetrically coordinated to the metal (difference in metal−carbon distances is about 0.1 Å) and exhibits in-plane coordination. The chain is turned in such a way that the α-agostic bond is anti with respect to the olefin. The Zr−H_{ag} bond is shorter than that found for the α-H agostic resting state **II** (by 0.145 Å) whereas the corresponding Zr−C_α bond is a little longer in **VIII** (by 0.025 Å). The metal−C_α−C_β angles are comparable in the two complexes.

Let us consider now the possible reaction steps connecting the β-H complexes (**III** and **IV**) to the α-H complexes (**VII** and **VIII**). It is useful to first compare the structures of these compounds with those previously reported.[50] Indeed, **III** and **VIII** present characteristics similar to those of the β-H syn and α-H species proposed by Lohrenz et al.[50] Hence, calculations were performed to locate a transition structure connecting **III** and **VIII**. However, no saddle point connecting these structures was found despite different initial conditions tried. This suggests that the FS mechanism must involve different reaction steps not yet described in the literature. Thus, transition structures connecting different intermediates were systematically searched. Since structure **VII** presents the characteristic of having the olefin in an approximately perpendicular position with respect to the symmetry plane of the Cp ligands, it could be formed either from the β-H syn complex **III** (by a concerted rotation of the monomer and the chain) or from the β-H syn ⊥ complex **IV** (by rotation of the chain). Similarly, transformations of **III** into **IV** and of **VII** into **VIII** (through rotation of the olefin in both cases) appear to be good candidates for a TS search. However, only two TS structures, **IX** and **X** (see Figure 6), were located corresponding to processes connecting **IV** to **VII** and **VII** to **VIII**, respectively. All the other TS calculations found no further saddle points.

The transition structure **IX** is close to the intermediate **VII**. In particular, the Zr−C_α and Zr−olefin distances are similar. The main difference lies in the rotation angle of the chain (the X−Zr−C_α−C_β dihedral angles, where X is the midpoint between olefin carbon atoms, are 41.4° in **IX** and 54.4° in **VII**).

In transition structure **X**, the olefin turns toward in-plane coordination whereas the chain continues its rotation around the Zr−C_α bond, the α-agostic interaction being enhanced (Zr−H_{ag} = 2.584 Å, Zr−C_α−H_{ag} = 87.4°). As a consequence, the distance between the C_α atom and the C_2 atom in the olefin decreases notably.

We can conclude that, in the earliest stages of the reaction, the FS process requires the formation of the perpendicular β-H syn ⊥ π-complex **IV**. Afterward, the reaction proceeds through a rotation of the monomer and polymer chain to reach a structure which favors the monomer insertion. This rotation mechanism is in fact a two-step process which can be basically schematized by chain rotation (**IV** to **VII**) followed by monomer rotation (**VII** to **VIII**).

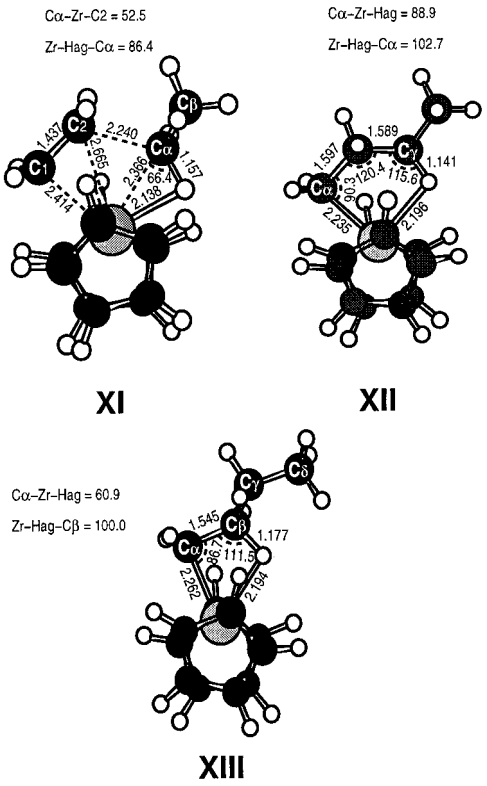

Figure 7. Transition structure for insertion (**XI**) and products, γ-H (**XII**) and β-H (**XIII**), in the FS mechanism.

The perpendicular complexation has not been previously proposed in the literature. As we shall comment below, the corresponding complex **IV** is a little less stable than the in-plane complex **III** but, according to the present results, its formation is a necessary step toward insertion. Indeed, the perpendicular complexation is compatible with the results of Car−Parrinello molecular dynamics simulations[52] which showed that during the monomer-active species approach, the olefin rotates and adopts a more or less perpendicular orientation (see Figure 3B in ref 52). These simulations also suggested that the conversion of β-H agostic into α-H agostic complexes is quite easy and may occur along with the complexation step.

Insertion. Let us consider now the final step of the FS process, i.e., the insertion reaction from the α-H structure **VIII**. The transition structure **XI** connecting **VIII** to the product **XII** and this product are shown in Figure 7**.**

By comparing the geometry of these structures, one notes that several internal parameters are involved in the reaction coordinate, as expected since there are several bonds which are being formed or broken. The forming Zr−C_1 and C_2−C_α bonds in the transition structure **XI** are shortened by 0.335 and 0.599 Å with respect to their values in **VIII** and are 0.179 and 0.651 Å longer than in product **XII**. One may also note that in **XI** the C_1−C_2−C_α−H atoms lie in the same plane. A quite remarkable peculiarity is the short Zr−H_{ag} bond length (2.138 Å) predicted for this structure, which is the smallest observed in this study. This strong agostic interaction contributes to an increase in the electrophility of C_α and appears to be a fundamental factor in the activation of the insertion step, i.e., in the formation of the new C_α−C_2 bond.

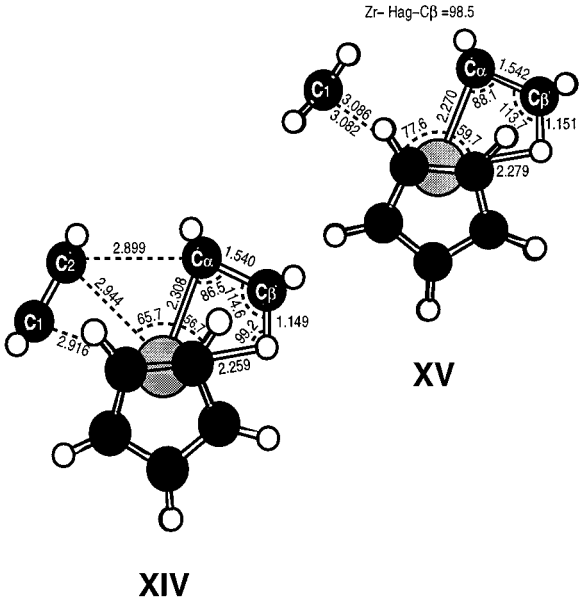

Figure 8. Main possible starting π-complexes for BS and SBS mechanisms: β-H anti (**XIV**) and β-H anti $\perp$ (**XV**).

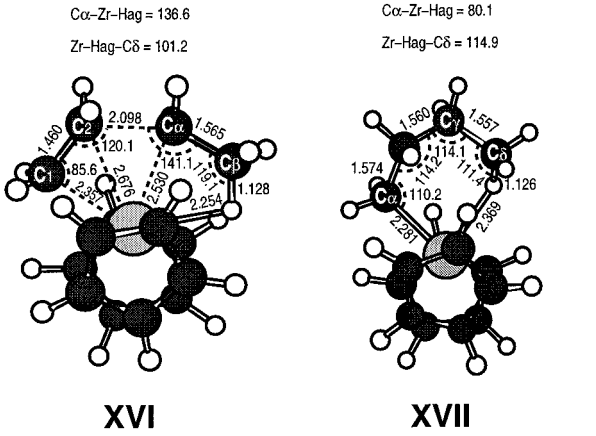

Figure 9. Transition structure (**XVI**) and δ-H product (**XVII**) in the BS mechanism.

After insertion, the corresponding product, **XII**, displays a γ-agostic interaction with a bond length intermediate between the values predicted for the resting states β-H (**I**) and α-H (**II**). Note that the angle $C_\alpha-C_\beta-C_\gamma$ (120.4°) is substantially larger than the value expected for an sp^3 C_β atom. Similarly, the $Zr-C_\alpha-C_\beta$ angle is rather small (90.3°). The carbon atoms of the chain are kept planar ($C_\alpha-C_\beta-C_\gamma-C_\delta = 181.91°$), but the planarity of $C_\alpha-C_\beta-C_\gamma-H$ (i.e., the $C_1-C_2-C_\alpha-H$ in structure **VIII**) is lost (dihedral angle of 61.3°).

The chain in the γ-H product **XII** can easily reorganize to yield the more stable β-H resting state, **XIII**. The structure of the final product is depicted in Figure 7. Compared to the previous β-H resting state **I**, the β-H product (**XIII**) exhibits a shorter $Zr-H_{ag}$ bond and larger $Zr-C_\alpha$ and $C_\alpha-H_{ag}$ distances. Clearly, the growing polymer chain has an important effect on the properties of the metal−chain bonds which may be related to its donor properties (see below, however). This effect appears to strengthen the interaction between the metal and the agostic hydrogen atom, in particular. The $Zr-C_\alpha-C_\beta-H_{ag}$ ring remains in a nearly planar conformation ($Zr-C_\alpha-C_\beta-H_{ag} = -8.9°$).

3.3. Backside Mechanism (BS). *Complexation.* As already described for the syn attack (FS mechanism), the anti attack of the olefin on the β-H resting state **I** proceeds with the formation of two possible species depending on the orientation of the olefin with respect to the original symmetry plane. These two species will be called hereafter β-H anti (**XIV**) and β-H anti $\perp$ (**XV**) and are depicted in Figure 8.

In **XIV**, the Zr, C_α, C_β, and H_{ag} atoms remain in the plane after the complexation. The Zr−olefin and $Zr-H_{ag}$ distances are shorter in **XIV** than in **III**. However, the $Zr-H_{ag}$ distance is longer than that in the resting state **I**. The symmetry of the structure is close to C_s.

In **XV**, the planarity of the $Zr-C_\alpha-C_\beta-H_{ag}$ ring is preserved too, so that the symmetry of the structure is almost C_s. The olefin is nearly perpendicular to the symmetry plane, and the $Zr-C_1$ and $Zr-C_2$ distances are very close. The $Zr-H_{ag}$ bond is slightly longer than that in the previous β-H anti complex (**XIV**).

Insertion. After formation of the β-H anti complex **XIV**, there is a single-step process leading to the product, which has a δ-agostic interaction. The corresponding TS (**XVI**) and product (**XVII**) are described in Figure 9.

The transition structure (**XVI**) still presents a relatively strong agostic bond (2.254 Å). The forming C_2-C_α bond is much shorter than that in the FS insertion TS. One may also remark that the bond angles in the forming six-membered ring $Zr-C_1-C_2-C_\alpha-C_\beta-H_{ag}$ are quite constrained.

The δ-H product (**XVII**) exhibits the largest agostic bond (2.369 Å) of the series of structures shown here. The conformation of the six-membered cycle resembles a chair cyclohexane. In other words, the rearrangement occurring after the insertion is substantial, since in the transition structure only one atom has moved out of the plane. To complete the catalytic cycle, **XVII** must rearrange to the γ-H (**XII**) and β-H (**XIII**) products described for the FS reaction.

3.4. Stepwise Backside Mechanism (SBS) Complexation. The starting point in this mechanism is the same as in the BS one, i.e., complexation to yield a β-H anti π-complex. However, instead of insertion, one may imagine a reaction path in which this complex undergoes a chain rearrangement so that the β-agostic bond is broken and an α-agostic complex is obtained, as in the FS mechanism. This rearrangement could lead in principle to the complex **VII** or **VIII**. A search for a TS connecting **XIV** or **XV** to either **VII** or **VIII** was unsuccessful. Nevertheless, a stepwise mechanism allowing us to go from **XIV** to **VII** has been predicted. This stepwise process is described below. The final part of the SBS mechanism is therefore the same as that of the FS mechanism explained above: **VII** → **VIII** → **XII** → **XIII**.

Chain Rearrangement. First, there is formation of complex **XIX** from **XIV** through the TS **XVIII**. These new structures are shown in Figure 10. In this step, the β-H bond is broken, giving two α-H bonds. No agostic bonds are found in the transition structure (**XVIII**). In this transition structure, C_α adopts a regular hybridization ($Zr-C_\alpha-C_\beta = 106.9°$). Complex **XIX** displays a very large $Zr-C_\alpha-C_\beta$ angle (132.7°) close to the one observed in the α-H complex **VIII**. Regarding the $Zr-H_\alpha$ distances (2.615 and 2.684 Å), we note the presence of two weak α-H interactions so that this species can be described as a double α-H complex [noted as a $(\alpha\text{-H})_2$ π-complex]. One should note that the Cp ligands in **XVIII** and **XIX** are almost staggered.

In a second step, the reaction proceeds from **XIX** to **VII**. It can be seen that these two intermediate complexes differ by rotation of the monomer, chain, and Cp ligands. The TS predicted by our computation **XX** is represented in Figure 10 and shows the monomer and the chain in their approximately

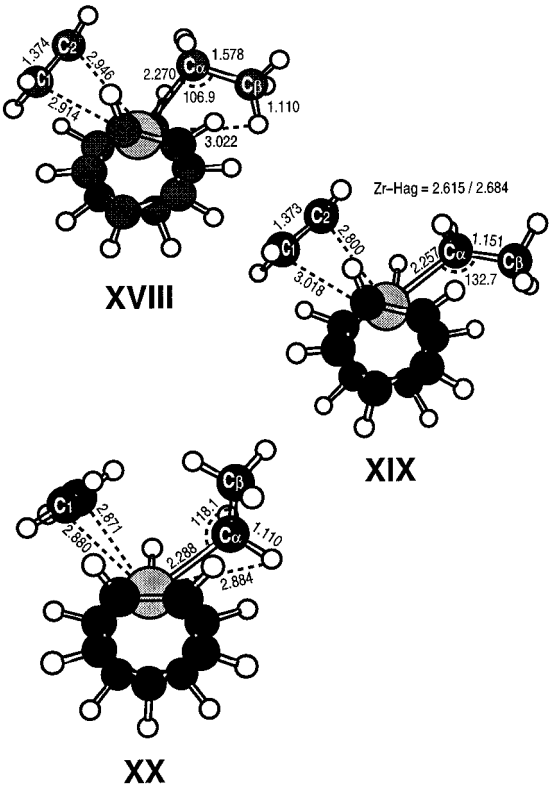

Figure 10. Structures involved in the SBS mechanism chain rearrangement step: transition hystructure for β-H bond breaking (**XVIII**), (α-H)$_2$ π-complex (**XIX**), and transition structure for olefin and chain rotation (**XX**).

TABLE 1: Energies of the Reactants

reactants		energies (kcal/mol)
β-H resting state	**I**	−321 489.12
α-H resting state	**II**	−321 481.35
ethylene		−49 277.89

final configuration, whereas the Cp ligands are basically unchanged with respect to the **XIX** starting structure.

4. Energetics

The total energies for the reactants are gathered in Table 1. Our calculations show that the α-H conformation **II** is 7.77 kcal/mol higher in energy than the β-H species **I**. This agrees with previous works[50] and justifies the hypothesis that the whole reaction mechanism starts with complexation of the monomer to the β-H resting state **I**. This complexation is very exothermic, since the active species is a cation and the olefin is an electron donor. It has been shown[67] that the coordination of the olefin to the β-H resting state proceeds downhill without any energy barrier. Linear transit calculations for a similar system,[68] but with a model chain of four carbon atoms, showed that γ-H and δ-H agostic π-complexes are formed without any barrier also. Finally, as we have shown above, the complexation does not dramatically affect the geometry of the initial species. Consequently, we did not try to analyze in detail the potential energy surface corresponding to the complexation step, assuming that it is an easy reaction, essentially barrierless.

The relative stabilities of all the structures computed is this work are summarized in Table 2. As shown, the most stable active species−monomer complex is **XIV**, the starting structure for BS and SBS mechanisms. The next complex in increasing order of energy is **III**, which was assumed to be the reactive species in the FS mechanism reported previously.[50] However, we have shown that it is not possible to connect this complex with the α-agostic intermediates that allow monomer insertion. The adequate complex for the FS reaction is **IV**, which lies 2.08 kcal/mol over **XIV**. Thus, according to our results, there is a thermodynamic preference for the formation of complexes involved in BS and SBS mechanisms. We must now examine the energy profiles for these mechanisms.

TABLE 2: Energies of the Structures Located in the Present Work (Relative to I + Ethylene)

structure		relative energy (kcal/mol)
β-H syn complex	**III**	−8.28
β-H syn $\perp$ complex	**IV**	−6.56
(β-H)$_2$ complex	**V**	−7.44
(β-H)$_2$ $\perp$ complex	**VI**	−6.12
α-H complex	**VII**	−7.77
α-H complex	**VIII**	−6.33
TS of chain rotation	**IX**	−5.98
TS of olefin rotation	**X**	−6.28
TS of insertion	**XI**	−4.77
γ-H product	**XII**	−17.35
β-H product	**XIII**	−20.70
β-H anti complex	**XIV**	−8.63
β-H anti $\perp$ complex	**XV**	−5.97
TS of insertion	**XVI**	−0.31
δ-H product	**XVII**	−15.57
TS of β-H bond breaking	**XVIII**	−5.32
(α-H)$_2$ complex	**XIX**	−8.41
TS of rearrangement	**XX**	−6.48

The energy profiles for the three mechanisms considered, FS, BS, and SBS, are schematically represented in Figure 11.

The BS mechanism may be described as

$$\mathbf{I} + C_2H_4 \xrightarrow{\text{barrierless}} \mathbf{XIV} \xrightarrow{\Delta E^{\ddagger} = 8.1 \text{ kcal/mol}} \mathbf{XVII}$$

Clearly, the BS mechanism is not competitive, since the activation barrier for insertion is substantially larger than the activation energies found for the other mechanisms. This in agreement with other theoretical studies.[50]

The FS mechanism begins through complexation to yield **IV**, which is a very shallow minimum. Then, **IV** may be converted into **VII** through a very low energy barrier (0.6 kcal/mol). Structure **VII** yields **VIII** through rotation of the olefin ($\Delta E^{\ddagger}$ = 1.5 kcal/mol), and **VIII** yields the product through olefin insertion ($\Delta E^{\ddagger}$ = 1.6 kcal/mol). Again, structure **VIII** is a very shallow energy minimum. One should note that energies in Table 2 and Figure 11 do not include zero-point energy corrections (ZPEs), since we were not able to compute the vibrational frequencies of these large systems. Indeed, one may predict that ZPEs will be slightly higher for reaction intermediates than for transition structures due to the additional degrees of freedom. Accordingly the trend will be to render the shallow structures **IV** and **VIII** unstable in the enthalpy (or free energy) profile. Hence, practically, the FS mechanism may be described by two main steps. The first one consists of the complexation of the olefin, oriented perpendicularly to the symmetry plane of the active species, to the β-H resting state, yielding structure **VII**. Along this complexation step, which is essentially barrierless, there is a rotation of the chain, breaking the β-H agostic interaction and conveniently orientating the C_α orbitals for the insertion process. Afterward, **VII** is converted into the product via a rotation of the olefin which, by changing perpendicular to in-plane orientation, renders possible the interaction between the olefin C_2 and the chain C_α atoms and allows C−C bond

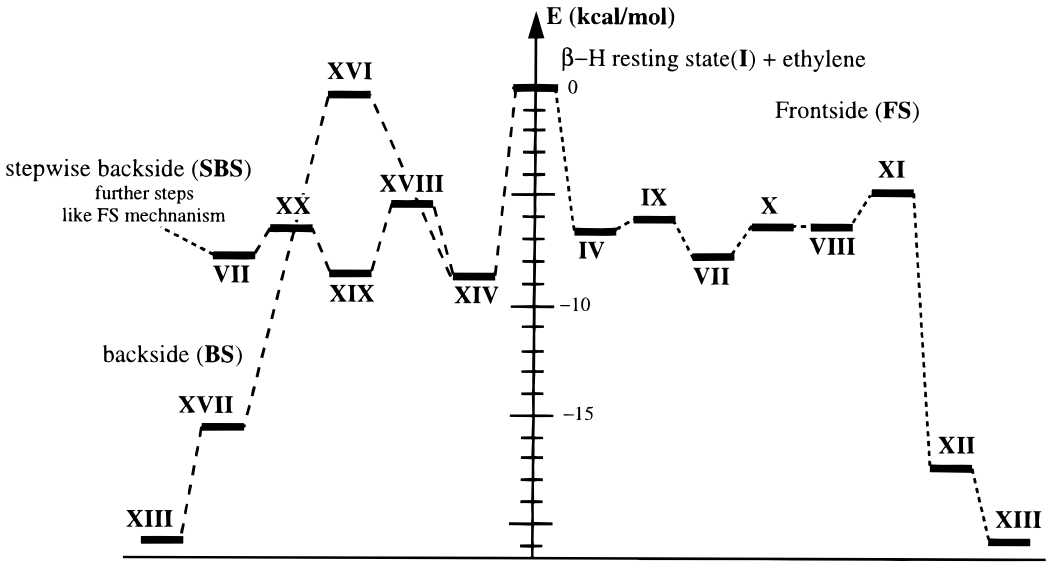

Figure 11. Energy profile for the three pathways predicted by our computations.

formation. In summary

$$\mathbf{I} + C_2H_4 \xrightarrow{\text{barrierless}} \mathbf{VII} \xrightarrow{\Delta E^{\ddagger} = 3.1 \text{ kcal/mol}} \mathbf{XII}$$

The computed activation energy for the insertion process is comparable to experimental (5[69] and 7.4[70] kcal/mole) and other theoretical values (3.2[71] and 5.6[72] kcal/mol) for related reactions.

This FS mechanism presents large differences from that previously reported.[50] We have already explained that this is due to the use of constrained geometry optimization in ref 50, in particular for locating a complex having an α-agostic bond and an in-plane coordination of the monomer (i.e., **VIII** in our work). Our results confirm the low stability of such a complex and put in evidence the crucial role played by the α-H complex **VII** in which the olefin is coordinated perpendicularly to the metal, which furnishes additional stabilization energy. The orientation of the olefin in the complexation step is therefore an important factor in the polymerization mechanism.

In the SBS mechanism, the first part of the reaction involves two well-differentiated steps. Complexation leads to the quite stable species **XIV**, which evolves through chain and monomer reorganization to yield **VII**. From here, the reaction proceeds as in the FS mechanism. Schematically, the SBS process may be written as

$$\mathbf{I} + C_2H_4 \xrightarrow{\text{barrierless}} \mathbf{XIV} \xrightarrow{\Delta E^{\ddagger} = 3.3 \text{ kcal/mol}} \mathbf{XIX} \xrightarrow{\Delta E^{\ddagger} = 1.9 \text{ kcal/mol}} \mathbf{VII} \xrightarrow{\Delta E^{\ddagger} = 3.1 \text{ kcal/mol}} \mathbf{XII}$$

According to these computations, the insertion mechanism in ethylene polymerization proceeds from structure **VII**, although there are two ways to reach this point from the reactants: a practically barrierless reaction (FS mechanism) or a stepwise process through prior formation of the thermodynamically most favorable complex **XIV** (SBS mechanism). The larger stability of **XIV** with respect to **VII** is not quite substantial (0.9 kcal/mol).

The energy differences between the FS and SBS mechanisms are small and are below the computational method accuracy. But one may expect these two mechanisms to be in competition in some cases depending on the precise nature of the catalysts or the experimental conditions. The size of the growing chain could also influence the energetics of the process. For instance, we have noted previously that the β-H bond in the resting state is stronger for the butyl than for the ethyl derivative. This may be expected to increase the barriers corresponding to the breaking of the β-H bond (**IV** to **VII** or **XIV** to **XIX**). Since such a process is the rate-limiting step of the SBS mechanism, increasing the chain size may be expected to favor the FS mechanism over the SBS mechanism.

5. Conclusions

A few theoretical papers have been already published on the mechanisms of ethylene polymerization catalyzed by metallocenes. Our results confirm some of the previously reported conclusions, in particular the essential role of agostic interactions along the reaction paths and the substantial preference for frontside (FS) with respect to backside (BS) insertion. However, our frontside mechanism is quite different from that proposed previously and, in addition, we show a new mechanism, called stepwise backside (SBS) insertion, which in some cases could be in competition with the frontside mechanism.

In our FS mechanism, the coordination of the olefin is made perpendicularly to the β-H resting state symmetry plane, which stabilizes the system and allows the chain to reorientate without any appreciable energy barrier. This result seems to be consistent with those of molecular dynamics trajectories. After complexation in this way, the insertion step is quite easy (about 3.0 kcal/mol). The predicted energy barrier is not far from theoretical values for equivalent reactions.[69−72]

The SBS, like the BS, mechanism begins through formation of the thermodynamically preferred monomer−active species complex which displays anti coordination of the in-plane olefin. In the BS mechanism, complexation is followed by direct insertion which requires a nonnegligible activation barrier (more than 8 kcal/mol). In the SBS mechanism, complexation is followed by a chain and monomer reorganization to yield, in a stepwise manner, the intermediate found in the FS mechanism, so that the insertion step is exactly the same. The reorganization requires, however, a small activation energy (3.3 kcal/mol for the largest barrier), which is of the same order of magnitude as that for the insertion step.

Modeling catalyzed reactions of experimental interest is still difficult considering the size of the systems involved. More simple models are thus necessary, but caution must be taken in order not to neglect important factors such as stabilization through agostic bonds or steric interactions. For instance, the

conclusions reached here for ethylene polymerization catalyzed by a simple metallocene species suggest that the mechanism of propylene polymerization can display large differences since, in this case, perpendicular complexation is less likely to occur. Substituents on the catalysts may also play a role. On the other hand, accurate computation on the simplest models will allow tests of the approximate computational techniques to study this industrially important class of chemical reactions.

Acknowledgment. We thank Dr. J. Malinge and Dr. T. Saudemont (Groupement de Recherches de Lacq, Elf Atochem) for helpful discussions and comments and Elf Aquitaine for authorizing publication of this work.

References and Notes

(1) Ziegler, K.; Holzkamp, E.; Breil, H.; Martin, H. *Angew. Chem.* **1955**, *67*, 541.
(2) Natta, G.; Pino, P.; Corradini, P.; Danusso, F.; Mantica, E.; Mazzanti, G. *J. Am. Chem. Soc.* **1955**, *77*, 1708.
(3) Cossée, P. *J. Catal.* **1964**, *3*, 80.
(4) Arlman, E. J. *J. Catal.* **1964**, *3*, 89.
(5) Arlman, E. J.; Cossée, P. *J. Catal.* **1964**, *3*, 99.
(6) Brookhart, M.; Green, M. L. H. *J. Organomet. Chem.* **1983**, *250*, 395.
(7) Andersen, A.; Cordes, H.-G.; Herwig, J.; Kaminsky, W.; Merck, A.; Mottweiler, R.; Pein, J.; Sinn, H.; Vollmer, H. J. *Angew. Chem., Int. Ed. Engl.* **1976**, *15*, 630.
(8) Johnson, L. K.; Killian, C. M.; Brookhart, M. *J. Am. Chem. Soc.* **1995**, *117*, 6414.
(9) Johnson, L. K.; Mecking, S.; Brookhart, M. *J. Am. Chem. Soc.* **1996**, *118*, 267.
(10) Killian, C. M.; Tempel, D. J.; Johnson, L. K.; Brookhart, M. *J. Am. Chem. Soc.* **1996**, *118*, 11664.
(11) Brintzinger, H. H.; Fischer, D.; Müllhaupt, R.; Rieger, B.; Waymouth, R. M. *Angew. Chem., Int. Ed. Engl.* **1995**, *34*, 1143.
(12) Alelynuas, Y. W.; Jordan, R. F.; Echols, S. F.; Borkowsky, S. L.; Bradley, P. K. *Organometallics* **1991**, *10*, 1406.
(13) Gassmann, P. G.; Callstrom, M. R. *J. Am. Chem. Soc.* **1987**, *109*, 7875.
(14) Jordan, R. F.; Bajgur, C. S.; Willett, R.; Scott, B. *J. Am. Chem. Soc.* **1986**, *108*, 7410.
(15) Gao, J. *Rev. Comput. Chem.* **1996**, *7*, 119. (b) Ruiz-López, M. F.; Rivail, J. L. In *Encyclopedia of Computational Chemistry*; Schleyer, P. v. R., Ed.; Wiley & Sons: New York; in press.
(16) Deng, L.; Woo, T. K.; Cavallo, L.; Margl, P. M.; Ziegler, T. *J. Am. Chem. Soc.* **1997**, *119*, 6177.
(17) Castongué, L. A.; Rappé, A. K. *J. Am. Chem. Soc.* **1992**, *114*, 5832.
(18) Siegbahn, P. E. M. *Chem. Phys. Lett.* **1993**, *205*, 290.
(19) Bierwagen, E. P.; Bercaw; J. E.; Goddard, W. A., III. *J. Am. Chem. Soc.* **1994**, *116*, 1481.
(20) Weiss, H.; Ehrig, M.; Ahlrichs, R. *J. Am. Chem. Soc.* **1994**, *116*, 4919.
(21) Meier, R. J.; van Dormemaele, G. H. J.; Iarlori, S.; Buda F. *J. Am. Chem. Soc.* **1994**, *116*, 7274.
(22) Fusco, R.; Longo, L. *Macromol. Symp.* **1995**, *89*, 197.
(23) van Dormemaele, G. H. J.; Meier, R. J.; Iarlori, S.; Buda F. *THEOCHEM* **1996**, *363*, 269.
(24) Cruz, V. L.; Muñoz-Escalona, A.; Martinez-Salazar, J. *Polymer* **1996**, *37*, 1163.
(25) Pietilä, L.-O.; Ahjopalo, L. *VTT Symp.* **1996**, *163*, 163.
(26) Cavallo, L.; Guerra, G. *Macromolecules* **1996**, *29*, 2729.
(27) Bierwagen, E. P.; Goddard, W. A., III. *Polym. Mater. Sci. Eng.* **1996**, *74*, 364.
(28) Fan, L.; Krzywicki, A.; Somogyvari, A.; Ziegler, T. *Inorg. Chem.* **1996**, *35*, 4003.
(29) Margl, P.; Ziegler, T. *J. Am. Chem. Soc.* **1996**, *118*, 7337.
(30) Margl, P.; Ziegler, T. *Organometallics* **1996**, *15*, 5519.
(31) Siegbahn, P. E. M.; Strömberg, S.; Zetterberg, K. *Organometallics* **1996**, *15*, 5542.
(32) Svensson, M.; Matsubara, T.; Morokuma, K. *Organometallics* **1996**, *15*, 5568.
(33) Deng, L.; Margl, P.; Ziegler, T. *J. Am. Chem. Soc.* **1997**, *119*, 1094.
(34) Musaev, D. G.; Froese, R. D. J.; Svensson, M.; Morokuma, K. *J. Am. Chem. Soc.* **1997**, *119*, 367.
(35) Musaev, D. G.; Svensson, M.; Morokuma, K.; Strömberg, S.; Zetterberg, K.; Siegbahn, P. E. M. *Organometallics* **1997**, *16*, 1933.
(36) Prosenc, M.-H.; Brintzinger, H.-H. *Organometallics* **1997**, *16*, 3889.
(37) Kawamura-Kuribayashi, H.; Koga, N.; Morokuma, K. *J. Am. Chem. Soc.* **1992**, *114*, 2359.
(38) Kawamura-Kuribayashi, H.; Koga, N.; Morokuma, K. *J. Am. Chem. Soc.* **1992**, *114*, 8687.
(39) Koga, N.; Yoshida, T.; Morokuma, K. In *Ziegler Catalysis*; Furk, G., Mülhaupt, R., Brintzinger, H. H., Eds.; Springer: Berlin, 1995; pp 277−289.
(40) Yoshida, T.; Koga, N.; Morokuma, K. *Organometallics* **1995**, *14*, 746.
(41) Yoshida, T.; Koga, N.; Morokuma, K. *Organometallics* **1996**, *15*, 766.
(42) Koga, N.; Yoshida, T.; Morokuma, K. *Polym. Mater. Sci. Eng.* **1996**, *74*, 360.
(43) Morokuma, K.; Yoshida, T.; Koga, N.; Musaev, D. G. *Polym. Mater. Sci. Eng.* **1996**, *74*, 425.
(44) Woo, T. K.; Fan, L.; Ziegler, T. *Organometallics* **1994**, *13*, 432.
(45) Woo, T. K.; Fan, L.; Ziegler, T. *Organometallics* **1994**, *13*, 2252.
(46) Woo, T. K.; Fan, L.; Ziegler, T. In *Ziegler Catalysis*; Furk, G., Mülhaupt, R., Brintzinger, H. H., Eds; Springer: Berlin, 1995; pp 293−315.
(47) Fan, L.; Harrison, D.; Deng, L.; Woo, T. K.; Swerhone, D.; Ziegler, T. *Can. J. Chem.* **1995**, *73*, 989.
(48) Fan, L.; Harrison, D.; Deng, L.; Woo, T. K.; Ziegler, T. *Organometallics* **1995**, *14*, 2018.
(49) Lohrenz, J. C.; Woo, T. K.; Fan, L.; Ziegler, T. *J. Organomet. Chem.* **1995**, *497*, 91.
(50) Lohrenz, J. C.; Woo, T. K.; Ziegler, T. *J. Am. Chem. Soc.* **1995**, *117*, 12973.
(51) Woo, T. K.; Margl, P. M.; Lohrenz, J. C. W.; Böchl, P. E.; Ziegler, T. *J. Am. Chem. Soc.* **1996**, *118*, 13021.
(52) Margl, P.; Lohrenz, J. C. W.; Ziegler, T.; Blöchl, P. E. *J. Am. Chem. Soc.* **1996**, *118*, 4434.
(53) Lohrenz, J. C. W.; Woo, T. K.; Fan, L.; Harrison, D.; Margl, P.; Ziegler, T. *Polym. Mater. Sci. Eng.* **1996**, *74*, 391.
(54) Woo, T. K.; Margl, P. M.; Lohrenz, J. C. W.; Ziegler, T. *Polym. Mater. Sci. Eng.* **1996**, *74*, 393.
(55) Woo, T. K.; Margl, P. M.; Ziegler, T.; Blöchl, P. E. *Organometallics* **1997**, *16*, 3454.
(56) Cavallo, L.; Guerra, G.; Corradini, P. *J. Am. Chem. Soc.*, **1998**, *120*, 2438.
(57) Brookhart, M.; Green, M. L. H. *J. Organomet. Chem.* **1983**, *250*, 395.
(58) Grubbs, R. H.; Coates, G. W. *Acc. Chem. Res.* **1996**, *29*, 85.
(59) Frisch, M. J.; Trucks, G. W.; Schlegel, H. B.; Gill, P. M. W.; Johnson, B. G.; Robb, M. A.; Cheeseman, J. R.; Keith, T.; Petersson, G. A.; Montgomery, J. A.; Raghavachari, K.; Al-Laham, M. A.; Zakrzewski, V. G.; Ortiz, J. V.; Foresman, J. B.; Peng, C. Y.; Ayala, P. Y.; Chen, W.; Wong, M. W.; Andres, J. L.; Replogle, E. S.; Gomperts, R.; Martin, R. L.; Fox, D. J.; Binkley, J. S.; Defrees, D. J.; Baker, J.; Stewart, J. P.; Head-Gordon, M.; Gonzalez, C.; Pople, J. A. *Gaussian 94*, Revision D.3; Gaussian, Inc.: Pittsburgh, PA, 1995.
(60) Dunning, T. H., Jr.; Hay, P. J. In *Modern Theoretical Chemistry*; Schaefer, H. F., III, Ed.; Plenum: New York, 1976; pp 1−28.
(61) Hay, P. J.; Wadt, W. R. *J. Chem. Phys.* **1985**, *82*, 270.
(62) Wadt, W. R.; Hay, P. J. *J. Chem. Phys.* **1985**, *82*, 284.
(63) Hay, P. J.; Wadt, W. R. *J. Chem. Phys.* **1985**, *82*, 299.
(64) Becke, A. D. *Phys. Rev. A* **1988**, *38*, 3098. (b) Lee, C.; Yang, W.; Parr, R. G. *Phys. Rev. B* **1988**, *37*, 785.
(65) Peng, C.; Schlegel, H. B. *Isr. J. Chem.* **1993**, *33*, 449.
(66) Eisenstein, O.; Jean, Y. *J. Am. Chem. Soc.* **1985**, *107*, 1177.
(67) Footnote 36 in ref 40.
(68) Woo, T. K.; Margl, P. M.; Lohrenz, J. C. W.; Blöchl, P. E.; Ziegler, T. *J. Am. Chem. Soc.* **1996**, *118*, 13021.
(69) Activation energy for ethylene polymerization catalyzed by $CpZrCl_3$: Chien, J. C. W.; Wang, B.-P. *J. Polym. Sci., Polym. Chem. Ed.* **1990**, *28*, 15.
(70) Activation energy for ethylene polymerization catalyzed by (NM-Cp)$ZrCl_2$ (NM = neomenthyl): Chien, J. C. W.; Razavi, A. *J. Polym. Sci., Polym. Chem. Ed.* **1988**, *26*, 2369.
(71) RMP2 optimization with the larger basis set in ref 40.
(72) B3LYP calculations with triple-ζ quality basis in ref 25.